Bull. Astr. Soc. India (2006) **34**, 141–152

Probing stellar evolution with open star clusters

Jasonjot Singh Kalirai*
University of California Observatories/Lick Observatory, University of California at Santa Cruz, 1156 High Street, Santa Cruz, California 95064, USA

Abstract. We derive the age, distance, reddening, binary fraction, metallicity, and star formation rate for the rich open star cluster NGC 2099 by comparing a high quality observational colour-magnitude diagram (CMD) with synthetic CMDs based on MonteCarlo numerical simulations. This approach accounts for all of the main parameters which determine the shape of the CMD for a stellar population and, unlike theoretical isochrone fits, allows a detailed comparison of the number of stars in various evolutionary phases. The resulting parameters are a key input into determining how much mass stars in NGC 2099 have lost through post main-sequence evolution. We follow up our deep imaging study with multi-object spectroscopy of ∼20 cluster white dwarf stars and constrain the initial-final mass relationship. The results clearly indicate that stars with initial masses between 2.8 and 3.4 $M_{\odot}$ lose 70–75% of their mass through stellar evolution. For the first time, we find some evidence for a metallicity dependence on the initial-final mass relationship.

Keywords : colour-magnitude diagrams – open clusters and associations: individual (NGC 2099) – stars: evolution – techniques: spectroscopic – white dwarfs

1. Introduction

The relation between the initial mass of a main-sequence star and its final mass as a white dwarf (WD), for intermediate mass stars, is a fundamental input to several interesting astrophysical problems. For example, for the determination of the ages and distances of globular clusters from modelling their WD cooling sequences (Hansen et al. 2004),

*e-mail:jkalirai@ucolick.org

for constraining chemical evolution in galaxies, for determining supernova rates (van den Bergh and Tammann 1991) and for understanding feedback processes and star formation in galaxies (e.g., Somerville and Primack 1999). Yet, despite its fundamental importance, the initial-final mass relationship remains poorly constrained observationally.

Attempts to map the initial-final mass relationship have been made as early as 1977 (Weidemann 1977). The best methods require observing a sample of WDs in young open star clusters and then spectroscopically measuring masses for the WDs through the modelling of their hydrogen balmer absorption lines (Bergeron, Saffer, and Liebert 1992). These masses, combined with cooling models, directly yield the WD cooling age of the star. As they are cluster members, the difference between the age of the cluster and the cooling age yields the main-sequence lifetime of the progenitor star that created the WD (and hence the progenitor mass). Therefore, a key input into the determination of the initial-final mass relationship is an accurate age measurement for the cluster under investigation.

The Canada-France-Hawaii Telescope (*CFHT*) Open Star Cluster Survey (Kalirai et al. 2001a) has identified many rich open star clusters. NGC 2099 is a prime example of a very rich, nearby cluster with an intermediate age. In Kalirai et al. (2001b), we identified several thousand cluster members in NGC 2099 and derived its age by comparing the observed main sequence, turn-off, and red giant clump with a set of theoretical isochrones (Ventura et al. 1998). In this contribution, we refine the earlier age measurement by comparing the observed CMD with synthetic CMDs based on MonteCarlo simulations (see also Kalirai and Tosi 2004) and use this to constrain the initial-final mass relationship (see also Kalirai et al. 2005a).

2. Observations

Imaging and spectroscopic observations of NGC 2099 were obtained with the *CFHT*, *Gemini North*, and *Keck I* telescopes. In our wide field *CFHT* imaging study (see Kalirai et al. 2001b), we found $\sim$ 67 WD candidates in the central $15'$ of NGC 2099. The observations and data reduction of this data are presented in Kalirai et al. (2001b). Based on comparisons between the cluster field and a blank field surrounding the cluster, we estimate the rate of field star contamination amongst our candidates to be $\sim 25\%$ (thus yielding 50 cluster WD candidates). We then plotted the locations of all of these faint-blue objects on the sky and obtained further observations of 3 smaller sub-fields in the cluster. These fields were chosen to maximize the number of WD candidates (all objects in the faint-blue end of the CMD were treated as WD candidates). With *Gemini*, we imaged three $5.'5 \times 5.'5$ fields using the GMOS multi-object imaging/spectroscopic instrument. With *Keck*, we imaged the same three fields with the LRIS imaging/spectroscopic instrument which has a $5' \times 7'$ field of view. These imaging data were not significantly deeper than the original *CFHT* data and were only used to ensure astrometric accuracy for the spectroscopy.

Multi-object spectra were obtained for a single *Gemini* field, and for two of the *Keck* fields. The *Gemini* observations used the B600 grating which simultaneously covers 2760 (centered at $\sim$ 4700 Å). The data were binned by a factor of four in the spectral direction to improve the signal-to-noise ratio (S/N). The *Keck* observations use the 600/4000 grism (blue side) which simultaneously covers 2580 Å (centered at 4590 Å). For the *Gemini* field, we obtained 22 individual 1-hour exposures spread over 22 days, taken mostly at low air-masses (< 1.2) and good seeing ($\sim 0.''8$). For the *Keck* fields, we obtained 4 2000 s exposures in each of the two fields, also at sub-arcsecond seeing.

The *Gemini* spectroscopic data were reduced using the *Gemini* IRAF package, version 1.3. The *Keck* data were reduced using a set of python routines written by Dan Kelson (D. Kelson, 2004, private communication; Kelson 2003). The individual exposures were bias subtracted, flat-fielded, cleaned for cosmic rays, wavelength calibrated, sky subtracted, extracted, combined, and flux calibrated (using bright standard stars) within each of these programs. The only major problem occurred for some of the *Keck* field 2 spectra which were taken at high air-masses and so the bluest flux was lost due to atmospheric dispersion. Fortunately, two of the three stars which we are fitting from this field have also been observed in the higher S/N *Gemini* data.

In total, we obtained spectroscopy of 24 individual WD candidates in the field of NGC 2099 (3 of these stars turned out not to be WDs). Therefore, despite sampling only 14% of the total cluster area, we include almost 1/3 of the total WD population (cluster and field) given the careful positioning of the fields. This is therefore the largest individual star cluster WD sample that has ever been spectroscopically acquired. A colour-magnitude diagram (CMD) showing the locations of the NGC 2099 WDs is shown in Figure 1 (based on *CFHT* data). The larger red dots in the faint-blue end of the CMD represent those objects for which we obtained a spectra to confirm WD nature. All of the complete spectra are shown in Kalirai et al. (2005b).

3. Synthetic colour-magnitude diagrams

3.1 Background

As shown in Figure 1, the CMD of NGC 2099 exhibits a very well defined, long main-sequence of over 12 magnitudes. The turnoff, red giant clump, and evolution off the clump are also clearly seen. In the faint-blue end of the CMD, a large WD population is evident. We find that a theoretical isochrone of age 650 Myrs fits the observed cluster main-sequence well. For this age, we have used newly derived cluster metallicity ($Z = 0.011 \pm 0.001$) and reddening values ($E(B-V) = 0.23 \pm 0.01$ - Deliyannis et al. 2004, private communication). The isochrone shown was calculated by Ventura et al. (1998). We also derive similar ages using the Padova group (620 Myrs - Girardi et al. 2000) and Yale-Yonsei isochrones (630 Myrs - Yi et al. 2001) for this metallicity.

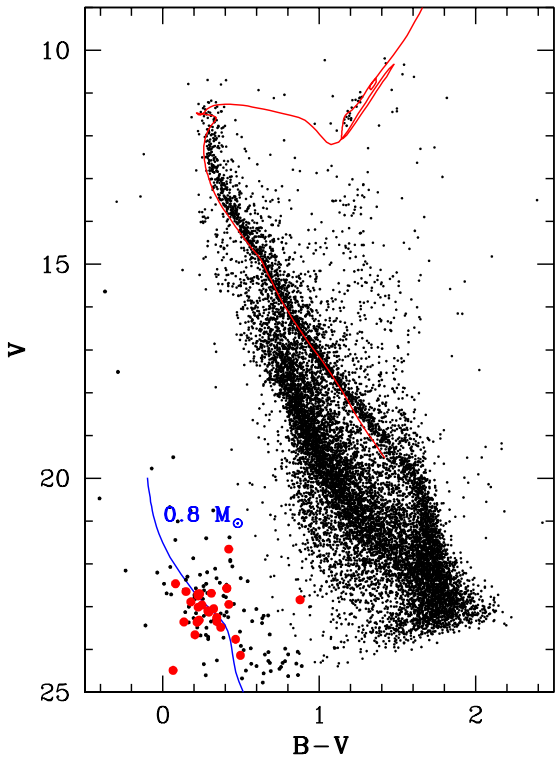

Figure 1. Rich, tight and long main-sequence of NGC 2099 is clearly separated from the background/foreground distribution. An isochrone of age 650 Myrs is overplotted on the NGC 2099 sequence and found to fit the observed photometry well. White dwarf targets that were spectroscopically observed are shown as larger red dots in the faint-blue end of the CMD. Also shown is a WD cooling model (Wood 1995) for $M = 0.8\ M_{\odot}$.

We now rederive the age for NGC 2099 by applying the synthetic CMD method (Tosi et al. 1991) to the empirical CMD described above. The best values of the parameters (including distance, age, binary fraction, etc.) are found by selecting the values that provide synthetic CMDs with morphology, number of stars in the various evolutionary phases and luminosity functions in better agreement with the empirical ones. The method has already been succesfully applied to several clusters (Bragaglia 2003 and references therein).

The synthetic CMDs are constructed via MonteCarlo extractions of (mass, age) pairs, according to an assumed IMF, SF law, and time interval of the SF activity. Each extracted

synthetic star is placed in the CMD by suitable interpolations on the adopted stellar evolution tracks and adopting the Bessell et al. (1998) tables for photometric conversion in the Johnson-Cousins photometric system. The absolute magnitude is converted to a *provisional* apparent magnitude by applying (arbitrary) reddening and distance modulus. The synthetic stars extracted for any magnitude and photometric band are assigned the photometric error derived for the actual stars of the same apparent magnitude. Then, they are randomly retained or rejected on the basis of the incompleteness factors of the actual data, derived from extensive artificial star tests.

Once the number of objects populating the whole synthetic CMD (or portions of it) equals that of the observed one, the procedure is stopped, yielding the quantitative level of the SF rate consistent with the observational data, for the prescribed IMF and SF law. To evaluate the goodness of the model predictions, we compare them with: the observational luminosity functions, the overall morphology of the CMD, the stellar magnitude and colour distributions, the number of objects in particular phases (e.g., on the red giant branch, in the clump, on the blue loops, etc.). A model can be considered satisfactory only if it reproduces all of the features of the empirical CMDs and luminosity functions. Given the uncertainties affecting both the photometry and the theoretical parameters (stellar evolution tracks included), the method cannot provide strictly unique results; however, it allows us to significantly reduce the range of acceptable parameters.

To estimate if, and how many, unresolved binary systems could be present in the cluster, the synthetic CMDs have been computed both assuming that all the cluster stars are single objects and that an (arbitrary) fraction of them are members of binary systems with random mass ratio. Again, the comparison of the resulting main-sequence morphology and thickness with the observed ones allows us to derive information on the most likely fraction of binaries.

3.2 The models

To test the effect of different input physics on the derived age, reddening and distance modulus, we have run the simulations with three different sets of stellar evolutionary tracks. The adopted sets were chosen because they assume different prescriptions for the treatment of convection and range from no overshooting to rather high overshooting from convective regions. Despite these differences, they are all able to well reproduce the observed CMDs of both star clusters and nearby galaxies. They are thus suitable to evaluate the intrinsic uncertainties still related to stellar evolution models. We use the FST tracks of Ventura et al. (1999) with high ($\zeta = 0.03$) and moderate ($\zeta = 0.02$) overshooting; the BBC94 tracks of the Padova group (Bressan et al. 1993; Fagotto et al. 1994), with overshooting; and the FRANEC tracks (Dominguez et al. 1999) with no overshooting. Incompleteness factors and photometric errors are taken from Kalirai et al. (2001b) and folded into the numerical simulations.

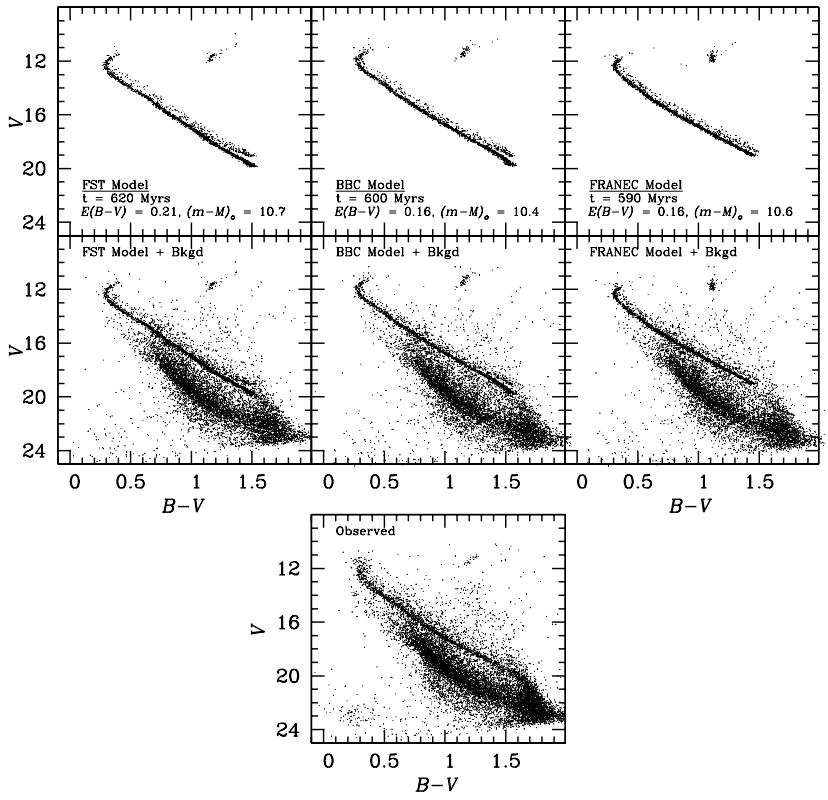

Figure 2. Synthetic CMDs for a 20% binary fraction (random mass ratio), are shown for NGC 2099. The BBC94 tracks are found to provide the best agreement with the observations (bottom panel). See §3.3 for more information.

All models assume that the star formation activity has lasted 5 Myr (i.e., approximately an instantaneous burst) and that the stars were formed following a single slope ($x = 1.35$) Salpeter's IMF over the whole mass range covered by the adopted tracks (0.6 – 100 $M_{\odot}$).

3.3 Results

The NGC 2099 cluster field contains 12194 *bona fide* stars, while a blank field surrounding the cluster, extrapolated to the cluster area, contains 10576 stars. Hence, the synthetic CMDs have been computed with 1618 objects.

In Figure 2 we present synthetic CMDs constructed from each of the FST, BBC94, and FRANEC models. For the FST (left), the synthetic sequences look impressively consistent with the observed one in all the minimal details. However, the turn-off and clump shape are not very good: the sequence after the turn-off is too long and curved and the clump is a bit short and faint. It is also very difficult to single out the best age, as anything between 520 and 700 Myrs doesn't significantly change the important CMD features (clump morphology and luminosity, shape of turn-off, etc...), all looking reasonable. The clump becomes too faint below 500 Myrs, indicating that this is a lower age limit and too blue beyond 800 Myrs indicating an upper limit. The best fit resulting parameters for these tracks are therefore age = 620 ± 60 Myrs, $E(B-V) = 0.21 \pm 0.02$, and $(m-M)_\circ = 10.70 \pm 0.20$. The BBC94 tracks (middle) excellently reproduce all of the main sequence and clump features, but have long post turn-off sequences, as we saw in the FST models. These tracks are in better agreement with the data than the FST models. The age is also better constrained, thanks to a higher sensitivity of the various features: age = 590 ± 10 Myrs, $E(B-V) = 0.18 \pm 0.01$, and $(m-M)_\circ = 10.50 \pm 0.10$. The FRANEC tracks (right) provide the best agreement with the observed upper main sequence and turn-off features. However, the resulting clump is too vertical and overpopulated. Part of the latter problem is due to the fact that their main sequence is not as deep as the others, because the minimum mass available to us is 0.7 $M_\odot$, instead of 0.6 $M_\odot$ as for the FST and Padova models. The code therefore can not distribute the required 1618 faint stars in these bins and, inevitably, puts a larger number of brighter stars according to a Salpeter IMF. The resulting best fit parameters in the FRANEC models are age = 590 ± 10 Myrs, $E(B-V) = 0.16 \pm 0.02$, and $(m-M)_\circ = 10.31 \pm 0.10$.

We have also perfomed several tests on the fraction of binary stars in NGC 2099. At first glance, the empirical CMD doesn't show any evidence of binaries, but we have found a posteriori that, without including them in the synthetic CMDs, both the turn-off morphology and the colour distribution on the red side of the main sequence are not well reproduced. Our best guess is that binaries are around 15-20% of the cluster stars and all of the results that we have discussed above assume this fraction (20%) with a random mass ratio.

Assuming a single slope Salpeter IMF, the mass of gas that formed the stars of the surveyed area of NGC 2099 between 0.6 and 100 $M_\odot$ is $\simeq 2.6 \times 10^3 M_\odot$ with the BBC94 models, $2.5 \times 10^3 M_\odot$ and $3.1 \times 10^3 M_\odot$ with the FST and the FRANEC models, respectively. For a distance of 1259 pc for NGC 2099, the surveyed area is 81 pc^2. The corresponding astrated mass per unit area is then 32.1 $M_\odot pc^{-2}$, equivalent to a star formation rate of 6.4×10^{-6} $M_\odot yr^{-1} pc^{-2}$. This values refers only to stars with masses included in the adopted sets of evolutionary tracks, namely from 0.6 to 100 $M_\odot$. To derive the total astrated mass and star formation rate, one should extrapolate down to 0.1 $M_\odot$, following the preferred IMF. In practice, extrapolating Salpeter's IMF down to 0.1 $M_\odot$, we must multiply by a factor 2.05 the astrated masses and the rates. If, at the other extreme, we prefer to assume the positive slope +0.44 below 0.6 $M_\odot$ suggested by Gould, Bahcall and Flynn (1997), then the above values must be multiplied only by 1.27.

4. The initial-final mass relationship

With well defined parameters for NGC 2099, we can now have a key input into deriving an initial-final mass relationship. As discussed earlier, we obtained multiobject spectroscopy of $\sim$ 20 WDs in NGC 2099 (see Kalirai et al. 2005b for spectra). Using the techniques described in Bergeron, Saffer, and Liebert (1992), we determine $T_{\rm eff}$ and log g for each WD. The line profiles are first normalized using two points on the continuum on either side of each absorption line. Therefore, the fit should not be affected by the flux calibration unless there is a strange "kink" or slope change at the location of a Balmer line. The fitting of the line shapes uses the nonlinear least-squares method of Levenberg-Marquardt (Press et al. 1986). The χ^2 statistic is calculated and minimized for combinations of $T_{\rm eff}$ and log g, using normalized model line profiles of all absorption lines simultaneously. The resulting 1-σ errors in $T_{\rm eff}$ and log g were tested by simulating synthetic spectra with the same number of absorption lines, and similar S/N, and measuring the output parameters from fitting these spectra. These results are found to have errors slightly less than those in the true spectra (as expected given small errors in flux calibration and other defects), and so we use the true spectra errors. Masses ($M_{\rm f}$) and WD cooling ages ($t_{\rm cool}$) are found by using the updated evolutionary models of Fontaine, Brassard, and Bergeron (2001) for thick hydrogen layers ($q({\rm H}) = M_{\rm H}/M = 10^{-4}$) and helium layers of $q({\rm He}) = 10^{-2}$. The core is assumed to be a 50/50 C/O mix. The model atmosphere fits for each WD are given in Kalirai et al. (2005a).

The WD cooling age represents the time that each of these stars has spent traversing from the tip of the AGB down to its present WD luminosity. We can now calculate the progenitor main-sequence lifetime ($t_{\rm ms}$, the total lifetime of the star up to the tip of the AGB) assuming an age for the cluster. The $t_{\rm ms}$ for each star is determined by subtracting the WD cooling ages ($t_{\rm cool}$) from the cluster age. The initial progenitor masses ($M_{\rm i}$) for the WDs are then calculated using the Hurley, Pols, and Tout (2000) models for Z = 0.01. For this metallicity, these models give very similar values to those derived from the Ventura et al. (1998) models. For these masses, a 100 Myr cluster age difference would only cause a $\sim$0.3 $M_{\odot}$ initial mass difference (for 350 Myr lifetimes). This is a very small effect on our initial-final mass relationship, and therefore the results are not highly sensitive to the derived cluster age.

In Figure 3 (top) we present the initial-final mass relationship for the sixteen WDs spectroscopically fit in this work (filled circles), as well as two other objects, WD6 and WD21 (see Kalirai et al. 2005b for the spectra of these objects). For these two stars, we could not determine an accurate log g due to the spectra having too low S/N. However, the effective temperatures are well constrained, and therefore, we derive the masses of the stars by combining this information with the luminosities (assuming they are cluster members). This gives the radius, which coupled with a mass-radius relation, gives the mass of the stars. The masses of these two stars, as well as their progenitor masses, are found to be in good agreement with others in the cluster (WD6 has $M_{\rm f}$ = 0.92 and $M_{\rm i}$ = 3.25, and WD21 has $M_{\rm f}$ = 0.85 and $M_{\rm i}$ = 3.13). Two of the WDs in our sample have

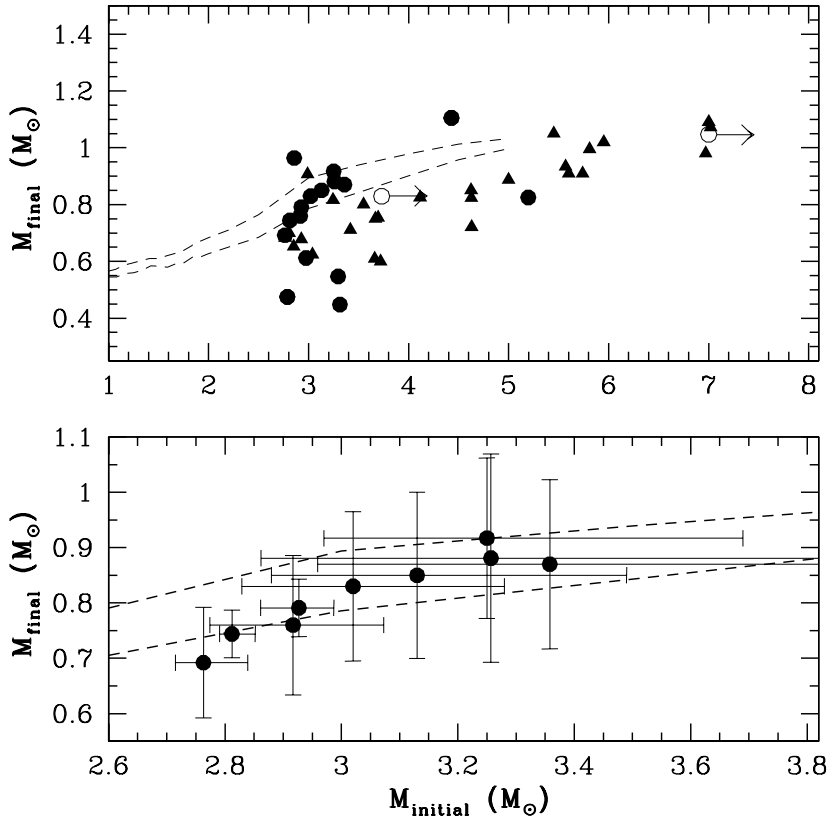

Figure 3. Top - the WD initial-final mass relationship is shown for the 18 WDs spectroscopically fit in this work (circles) and all previous constraints (triangles). Bottom - A closer look at those WDs that form the tight sequence with $M_{\rm i} = 2.8$–3.4 $M_\odot$, and bound by the two Marigo (2001) theoretical relations.

negative progenitor lifetimes. This is due to the WD cooling age of these stars being larger than the cluster age. For WD17, we artificially set its initial mass to 7 $M_\odot$ (the most massive star that produces a WD in the Ventura et al. 1998 models). For WD15, we compute a 95% confidence lower limit of 408 Myrs for $t_{\rm cool}$, and determine the initial mass based on this cooling age. These stars are both plotted with open circles and an arrow pointing to higher masses to reflect the lower limits. It is unlikely that these objects are field WDs given their unusually high masses (see Madej, Nalezyty, and Althaus 2004 for field WD mass distribution).

Figure 3 (top) shows that, with just one star cluster, we have nearly doubled the number of data points on the initial-final mass plane. This is remarkable considering

the time and effort required to establish the previous constraints (shown as triangles). Furthermore, half of our data points sit along a very tight sequence with initial masses in the range 2.8–3.4 $M_{\odot}$ and final masses in the range 0.7–0.9 $M_{\odot}$. Fitting these data points and their two dimensional errors to a straight line, we determine a slope of 0.33 and an intercept of -0.19. The residual rms of the fit is 0.03. This suggests that stars with masses between 2.8 and 3.4 $M_{\odot}$, and metallicities slightly less than Solar, will lose 70–75% of their mass through stellar evolution.

Four of our stars are seen well below the tight sequence of points discussed above. Although only one of these four stars has an inconsistent theoretical magnitude, they could still be field WDs located near the cluster. Not only are their masses consistent with the distribution of field WDs ($M = 0.56$ $M_{\odot}$ - Sloan Digital Sky Survey data - Madej, Nalezyty, and Althaus 2004), but we also expect 4-5 WDs in our sample to be field stars based on WD number counts in blank fields surrounding NGC 2099 (Kalirai et al. 2001b). The lower masses of these stars could also be attributed to binary star evolution and mass transfer. We will investigate these possibilities further in a future paper.

The two dashed lines in Figure 3 are theoretical initial-final mass relations from Marigo (2001), for $Z = 0.008$ (top) and $Z = 0.02$ (bottom). The latter models have improved mass-loss mechanisms in their post-main sequence evolutionary phases and therefore should be preferred over the others (L. Girardi, 2004, private communication). Considering this, it is interesting to note that half of our NGC 2099 cluster WDs reside in a region of the initial-final mass relationship bound by the two Marigo (2001) relations (see bottom panel of Figure 3). This is what we would expect, given that the cluster metallicity falls between that used in the two models ($Z = 0.011$). We point out however that the errors in our measurements are too large for us to be able to discriminate between the two relations. Our data points are, however, mostly located above the other previous constraints. This can also be explained by the fact that almost all of the other clusters are Solar or higher metallicity, resulting in more efficient mass loss during stellar evolution (Marigo 2001). Although this could be a systematic effect (e.g., the masses of the WDs in other clusters have been derived using different models), these results may be suggesting that, for the first time, we are seeing the effects of metallicity on the initial-final mass relationship.

The spectroscopic measurement of masses of WDs with $V \simeq 23$ has not been previously accomplished. The number of targets that are accessible at these magnitudes is several orders of magnitudes larger than previously identified. The already published work in the *CFHT* Open Star Cluster Survey (see Kalirai et al. 2001a; 2001b; 2001c; 2003), as well as clusters currently being observed will form the backbone of this study. In Figure 4 we present a sample of six of our richest open star clusters. Rich WD populations that can be spectroscopically studied are seen in all clusters (larger circles). With such data, we can envision placing >100 data points into this very fundamental relation. By observing both younger and older clusters (the six clusters in this Figure span an age

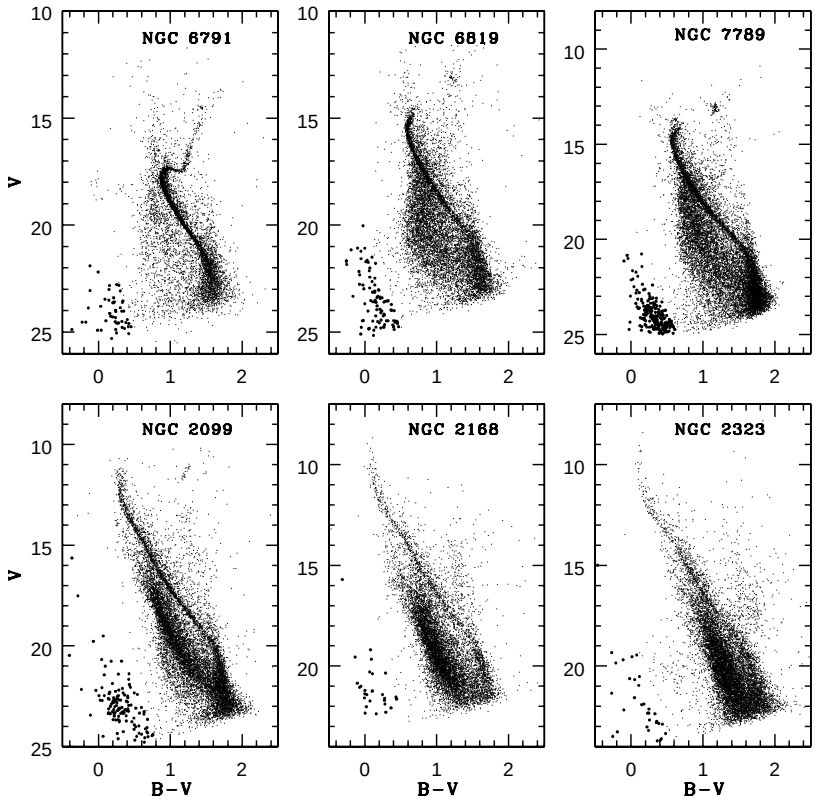

Figure 4. Six rich open star clusters, all observed as a part of the *CFHT* Open Star Cluster Survey, are shown in order of decreasing age. The oldest, NGC 6791 is 10 Gyrs old whereas the youngest, NGC 2323, is only 100 Myrs old. Rich WD populations in each cluster are highlighted with darker symbols. These stars will all be spectroscopically targeted in future observations to constrain the initial-final mass relationship for different mass ranges.

range of 100 Myrs – 10 Gyrs), the entire initial progenitor mass range can be constrained and a detailed initial-final mass relation can be produced.

Acknowledgements

The author would like to thank Monica Tosi for producing numerical simulations for this work and helping with interpretation of the model comparisons to the empirical CMDs. We are also greatly indebted to Pierre Bergeron for providing us with his models and spectral fitting routines, as well as for numerous discussions. Many thanks to David

Reitzel for helping reduce the *Keck* spectroscopic observations, and Paolo Ventura for providing updated theoretical isochrones.

References

Bergeron, P., Saffer, R. A., and Liebert, J., 1992, *ApJ*, **394**, 228.
Bessell, M. S., Castelli, F., and Plez, B., 1998, *A&A*, **333**, 231.
Bragaglia, A., 2003, in *Stars in Galaxies*, M. Bellazzini, A. Buzzoni, S. Cassisi eds, Mem.S.A.It. in press.
Bressan, A., Fagotto, F., Bertelli, G., and Chiosi, C., 1993, *A&AS*, **100**, 647.
Dominguez, I., Chieffi, A., Limongi, M., and Straniero, O., 1999, *ApJ*, **524**, 226.
Fagotto, F., Bressan, A., Bertelli, G., and Chiosi, C., 1994, *A&AS*, **105**, 29.
Fontaine, G., Brassard, P., and Bergeron, P., 2001, *PASP*, **113**, 409.
Girardi, L. et al., 2000, *A&AS*, **141**, 371.
Gould, A., Bahcall, J., and Flynn, C., 1997, *ApJ*, **482**, 913.
Hansen, B. M. S. et al., 2004, *ApJS*, **155**, 551.
Hurley, J. R., Pols, O. R., and Tout, C. A., 2000, *MNRAS*, **315**, 543.
Kalirai, J. S., Richer, H. B., Reitzel, D., Hansen, B. M .S., Rich, R. M., Fahlman, G. G., Gibson, B. K., and von Hippel, T., 2005a, *ApJL*, **618**, 123.
Kalirai, J. S., Richer, H. B., Hansen, B. M .S., Reitzel, D., and Rich, R. M., 2005b, *ApJL*, **618**, 129.
Kalirai, J. S. and Tosi, M., 2004, *MNRAS*, **351**, 649.
Kalirai, J. S., Fahlman, G. G., Richer, H. B., and Ventura, P., 2003, *AJ*, **126**, 1402.
Kalirai, J. S., Richer, H. B., Fahlman, G. G., Cuillandre, J., Ventura, P., D'Antona, F., Bertin, E., Marconi, G., and Durrell, P., 2001c, *AJ*, **122**, 266.
Kalirai, J. S., Ventura, P., Richer, H. B., Fahlman, G. G., D'Antona, F., and Marconi, G., 2001b, *AJ*, **122**, 3239.
Kalirai, J. S., Richer, H. B., Fahlman, G. G., Cuillandre, J., Ventura, P., D'Antona, F., Bertin, E., Marconi, G., and Durrell, P., 2001a, *AJ*, **122**, 257.
Kelson, D., 2003, *PASP*, **115**, 808, 688.
Madej, J., Nalezyty, M., and Althaus, L. G., 2004, *A&A*, **419**, L5.
Marigo, P., 2001, *A&A*, **370**, 194.
Press, W. H. et al., 1986, Numerical Recipes, Cambridge: Cambridge Univ. Press.
Somerville, R. S. and Primack, J. R., 1999, *MNRAS*, **310**, 1087.
Tosi, M., Greggio, L., Marconi, G., and Focardi, P., 1991, *AJ*, **102**, 951.
van den Bergh, S. and Tammann, G., 1991, *ARA&A*, **29**, 363.
Ventura, P., Zeppieri, A., Mazzitelli, I. and D'Antona, F., 1998, *A&A*, **334**, 953.
Weidemann, V., 1977, *A&A*, **59**, 411.
Wood, M. A., 1995, in Ninth European Workshop on White Dwarfs, NATO ASI Series, ed. D. Koester, and K. Werner (Berlin: Springer), 41.
Yi, S. et al., 2001, *ApJS*, **136**, 417.